MSDE

PAPER

View Article Online
View Journal | View Issue

Cite this: *Mol. Syst. Des. Eng.*, 2020, 5, 882

Heteroatom engineering of polymeric carbon nitride heterojunctions for boosting photocatalytic reduction of hexavalent uranium†

Fengtao Yu,‡[a] Zhiwu Yu,‡[b] Zhenzhen Xu,[a] Jianbo Xiong,[a] Qiangwen Fan,[a] Xuefeng Feng,[a] Yuan Tao,[a] Jianli Hua [c] and Feng Luo *[a]

Received 24th December 2019,
Accepted 17th February 2020

DOI: 10.1039/c9me00181f

rsc.li/molecular-engineering

Herein, for the first time, the authors report metal-free heterojunction photocatalysts consisting of push–pull conjugated polymers and polymeric carbon nitride (CN) for efficient reduction of uranium. Furthermore, the authors innovatively proposed a heteroatomic engineering strategy to further improve the visible-light capture ability and separation of electron–hole pairs of heterojunction photocatalysts *via* replacing carbon atoms in donors by nitrogen atoms. The result revealed that in the photocatalytic reduction of uranium, the kinetic constant of **PFB**/CN (0.037 min^{-1}) was 2.47 times higher than that of CN (0.015 min^{-1}). Notably, copolymerization of a nitrogen-containing electron donor carbazole unit into the polymer backbone would further widen the light response range and promote electron–hole separation within **PCB**/CN as compared to **PFB**/CN, leading to a higher kinetic constant (0.049 min^{-1}), 3.27 times higher than that of CN. The current work underlines that adapting a reasonable heteroatomic engineering strategy for polymer heterojunctions is a remarkably effective strategy to develop up-and-coming organic semiconductor photocatalysts for efficient reduction of uranium.

Design, System, Application

D–A conjugated copolymers have been reported to contain D-units and A-units that can push and pull the HOMO and LUMO energy levels to control the band structure. Moreover, the D–A conjugated copolymers with a π-conjugated structure can greatly improve the light absorption ability and simultaneously permit a high degree of intermolecular charge transfer. That is, two push–pull conjugated polymers termed as **PFB** and **PCB** with different donors (fluorene and carbazole) and benzothiadiazole as an acceptor unit were applied to fabricate **PFB**/g-C_3N_4 and **PCB**/g-C_3N_4 heterojunctions for efficient photocatalytic reduction of uranium. Moreover, the experimental results combined with the theoretical calculation results show that the donor based on carbazole containing a N heteroatom can work efficiently as a strongly electron donating site. As expected, the **PCB**/CN heterojunction has a wider visible spectrum absorption range and shows better activity for the photocatalytic reduction of uranium under visible light irradiation ($\lambda \geq 400$ nm). This rational molecular design strategy could offer a promising platform for developing efficient and stable polymer heterojunction photocatalysts for radionuclide removal and extraction.

Introduction

Uranium, a key element in the production of nuclear energy, has been widely used as a fission fuel and has made a significant contribution to solving the current global energy shortage.[1–3] However, large-scale uranium mining and processing, inadequate spent fuel reprocessing, and frequent nuclear accidents have led to the release of large amounts of uranium into the natural environment, which migrate into the ground or surface water systems as highly mobile hexavalent uranium(VI) ions.[4] Studies have shown that excessive uranium emission not only causes serious environmental pollution, but also brings serious health problems to humans.[5–8] Thus, how to effectively separate and recover uranium from wastewater has become a top priority.[9,10] At present, the reduction of U(VI) to hard to dissolve U(IV) oxides through semiconductor-based photocatalysts under sunlight irradiation has been considered to be a promising approach to eliminate uranium pollution.[11,12]

Polymeric carbon nitride (g-C_3N_4), as an emerging and metal-free two-dimensional polymer semiconductor with a fairly favourable light response, excellent physical–chemical properties and suitable electronic structure, has attracted significant attention in environmental photocatalytic

[a] *State Key Laboratory for Nuclear Resources and Environment, and School of Biology, Chemistry and Material Science, East China University of Technology, Nanchang, Jiangxi 344000, China. E-mail: ecitluofeng@163.com*
[b] *High Magnetic Field Laboratory, Chinese Academy of Sciences, Hefei 230031, Anhui, China*
[c] *Key Laboratory for Advanced Materials, Institute of Fine Chemicals, East China University of Science and Technology, 200237, Shanghai, China*

† Electronic supplementary information (ESI) available: Experiments and additional figures. See DOI: 10.1039/c9me00181f

‡ These authors have equally contributed to this work.

applications.[13–15] Unfortunately, the photoactivity of raw g-C_3N_4 is unsatisfactory because its visible light response above 460 nm is poor and photogenerated charge separation is not ideal.[16] In view of the above-mentioned shortcomings of unprocessed g-C_3N_4, many efficient methods have been devoted to optimize its band structures. For example, Lu *et al.* stated that U(VI) was reduced to U(IV) by boron or sulfur doped g-C_3N_4 under visible-light irradiation. By doping non-metal B or S, the visible light capturing ability of CN is improved, while the migration of the photogenerated carriers is promoted.[17,18] Recently, fabricating g-C_3N_4 based heterostructures for greatly promoting charge carrier separation efficiency and photocatalytic performance of pristine g-C_3N_4 have attracted enormous attention. According to different charge transfer mechanisms, the formed heterojunctions can be classified into three categories, and among them, the staggered-band-oriented heterojunction (type II) is the most reasonable structure to achieve effective electron–hole pair separation.[19–21] Notably, most of the current reports are g-C_3N_4/inorganic semiconductor heterojunctions. For instance, Sridharan *et al.* proved that the g-C_3N_4–TiO_2 heterojunction removes 33% Cr(VI) and 98% MB dye.[22] Nevertheless, the use of organic semiconductor/g-C_3N_4 heterojunctions for the reduction of hexavalent uranium has rarely been reported.

Inspired by g-C_3N_4, organic conjugated polymer semiconductor photocatalysts have also received much attention because of their wide visible-light absorption range, superior carrier fluidity and adjustable electronic structure.[23–27] Recently, donor–acceptor conjugated polymers manufactured by Cooper's team were also discovered to exhibit medium photocatalytic activity under visible-light irradiation.[28–32] In comparison with the most studied polymeric g-C_3N_4 with fairly regular structures, the abundance of donors and acceptors contributes to the adjustment of energy levels. As a result, the D–A type organic conjugated polymer semiconductors are considered to be a promising candidate for forming a type II heterojunction with g-C_3N_4.

Herein, for the first time, we have prepared D–A polymer/g-C_3N_4 heterojunctions for photocatalytic reduction of hexavalent uranium. Furthermore, we have innovatively proposed to improve the photocatalytic reduction of uranium in polymer heterojunctions through heteroatomic engineering strategies. To this end, two D–A conjugated polymers termed as **PFB** and **PCB** with different donors (fluorene and carbazole) and benzothiadiazole as an acceptor unit were applied to fabricate **PFB**/CN and **PCB**/CN heterojunctions. Both experimental and theoretical studies have shown that the donor based on carbazole containing a N heteroatom can work efficiently as a strongly electron donating site. As expected, **PCB** has a wider visible spectrum absorption range and the **PCB**/CN heterojunction shows better activity for the photocatalytic reduction of uranium under visible light irradiation ($\lambda \geq 400$ nm). After irradiation for 120 min, the removal efficiency for UO_2^{2+} over **PCB**/CN was 99.7%. In particular, the k value of **PCB**/CN was 0.049 min^{-1}, which was 3.27 times higher than that of g-C_3N_4 (0.015 min^{-1}). Moreover, for the purpose of gaining further understanding of the photocatalytic mechanism, a photoelectrochemical test, an XPS test and density functional theory (DFT) calculations were further implemented.

Results and discussion

D–A type conjugated polymers are expected to exhibit strong visible light absorption and effective Frenkel exciton dissociation owing to the occurrence of the push–pull intramolecular charge transfer (ICT). Thus, 2,7-dibromo-9,9-bis(2-ethylhexyl)-9*H*-fluorene was introduced as the donor, and a benzothiadiazole unit was used as the acceptor for the target polymer **PFB**. Moreover, in order to further facilitate the Frenkel exciton dissociation and enhanced sunlight capture capability, a carbazole donor having a stronger electron donating ability is obtained by substituting a nitrogen atom for a carbon atom linking the alkyl chain, then polymer **PCB** was obtained by a similar synthesis method. **PFB** and **PCB** were synthesized by classic Suzuki–Miyaura polymerization reactions (Scheme 1). Because the polymers contain flexible alkyl chains, they have good solubility in both THF and chloroform. Raw CN was obtained by directly heating urea in a muffle furnace. The polymer/CN photocatalysts were obtained quickly and easily through the intermolecular π–π interactions between aromatic-based conjugated **PFB** (**PCB**) and π-conjugated CN.

The chemical structures of the as-prepared solid specimens were characterized by powder X-ray diffraction (XRD, Fig. S1a†), Fourier transform infrared (FTIR) spectroscopy (Fig. S1b–d†), and X-ray photoelectron spectroscopy (XPS, Fig. S4†). From the XRD results, **PFB** and **PCB** are amorphous. The pristine CN displayed two distinct diffraction peaks at 13.0° and 27.2°, which correspond to the (100) and (002) planes of polymeric g-C_3N_4 (JCPDS#87-

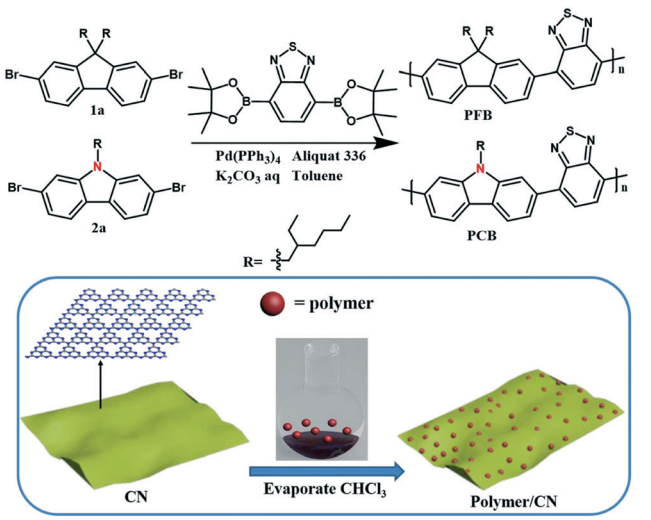

Scheme 1 General synthetic routes of **PFB**, **PCB** and polymer/CN.

1526).[33] Notably, the XRD patterns of **PFB**/CN and **PCB**/CN did not change significantly compared to that of CN, which means that the formation of a heterojunction does not affect their layered micromorphology. In the FTIR spectra, the raw CN exhibits typical characteristic peaks.[34] As for **PFB** and **PCB**, they exhibit strong transmittance because of their high rigidity. In order to clearly interpret the molecular structure of the polymers, the amplified infrared spectra are shown in Fig. S1c.† The absorption features observed at 1340 and 1520 cm^{-1} (the skeleton mode of the C=C group) in the spectra of **PFB** and **PCB** confirm the presence of aromatic rings. The representative stretching vibration peaks of S–N could also be found, which correspond to the absorption bands at 1610 and 1608 cm^{-1}. For polymer/CN, as the polymer mass ratio increases, the stretching of the C–N heterocycles and the bending vibration of the heptazine rings in CN become weaker (Fig. S1d, S2a and b†), which indicates the formation of intermolecular interactions between CN and the rigid conjugated polymers. X-ray photoelectron spectroscopy (XPS) was also undertaken to study carefully the surface chemical composition of the as-obtained samples (Fig. S4 and Tables S1–S4†), to further prove the successful preparation of the polymer heterojunctions. The morphology of CN, **PFB**, **PCB**, **PFB**/CN and **PCB**/CN was characterized by scanning electron microscopy (SEM). As displayed in Fig. S3,† **PFB** and **PCB** accumulated together into irregularly shaped particles. **PFB**/CN and **PCB**/CN exhibit a similar morphology (an irregular flake-like structure) to pristine CN, indicating that the formation of the heterojunction doesn't affect the main morphology and structure of the photocatalysts.[35–37]

UV-vis diffuse reflectance spectra (UV/vis DRS) were collected to investigate the optical absorption and band structure of all the as-prepared samples (Fig. 1). As seen from Fig. 1a, raw CN has a certain visible light absorbance but zero absorbance above 460 nm. **PFB** and **PCB** show excellent absorbance in the visible-light region. Compared to **PFB** (apparent color is dark yellow), **PCB** exhibited a clear red shift from ~566 nm to more than 610 nm with an orange red appearance, and the energy gaps (E_g) were calculated to be 2.22 eV and 2.07 eV for **PFB** and **PCB** from the Tauc plot fittings, respectively (Fig. 1b). The red-shift absorption periphery is attributed to the copolymerizing carbazole donor of **PCB** skeleton, which acquires stronger ICT from carbazole unit to benzothiadiazole acceptor. The extended absorption edge facilitates the use of visible light.[38,39]

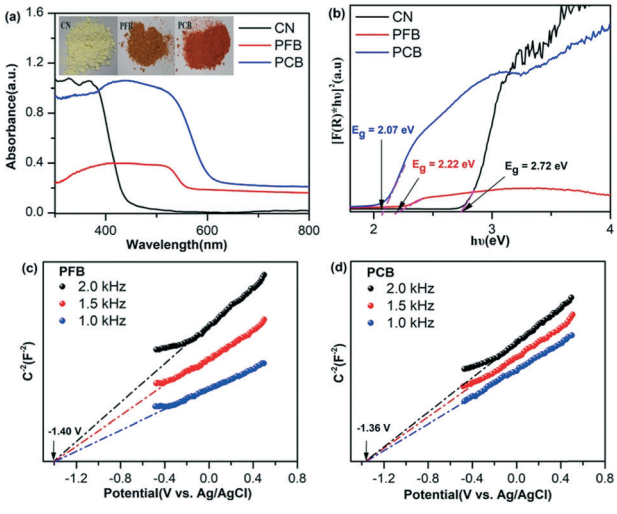

Fig. 1 (a) UV-vis diffuse reflectance spectra of CN, **PFB** and **PCB**; (b) the Tauc plots of **PFB** and **PCB**; (c) the Mott–Schottky (MS) plots of **PFB**; (d) the Mott–Schottky (MS) plots of **PCB**. The Mott–Schottky plots were recorded by using three different frequencies of the AC potential at 1000, 1500 and 2000 Hz.

The Mott–Schottky (MS) plots are utilized to evaluate the flat-band potential (E_{fb}) of CN, **PFB** and **PCB** in a 0.5 M Na_2SO_4 electrolyte at frequencies of 2.0, 1.5 and 1.0 kHz. As shown in Fig. 1c, d and S5,† CN, **PFB** and **PCB** all exhibit positive slopes in the C^{-2}–E plots, indicating the n-type property of the semiconductors.[40] The E_{fb} values of CN, **PFB** and **PCB** are −1.27 V, −1.40 V and −1.36 V *versus* Ag/AgCl, respectively. It is known that the conduction band potential (E_{CB}) for n-type semiconductors is the approximate flat band potential.[41] Thus, the E_{CB} values for CN, **PFB** and **PCB** are −1.27 V, −1.40 V and −1.36 V *versus* Ag/AgCl and −1.04 V, −1.17 V and −1.13 V *vs.* the standard hydrogen electrode (SHE), respectively. Furthermore, there is another valence band (E_{VB}) at about +1.68 V, +1.05 V and 0.94 V *vs.* SHE, respectively. It turns out that the copolymerized carbazole unit (having stronger electron-donating ability, Fig. S7†) in the polymer backbone increases E_{VB} and reduces the band gap, thereupon broadening the spectral absorption range. Notably, E_{CB} and E_{VB} of the polymers are much higher than those of CN. Thus, the band alignment between CN and **PFB** (**PCB**) suggests that it has a typical type II heterojunction structure.[42] This appropriate band-structure alignment between CN and the polymer creates a polarized built-in electric field at the interfaces, which is significant for effective photoelectron–hole pair separation.[43–47] The characterization results indicated that the as-prepared samples displayed the potential for the U(VI) photoreduction from aqueous solutions.

The activity of the polymer heterojunction photocatalysts for the photocatalytic reduction of uranium was methodically measured in the presence of 100 ppm UO_2^{2+} (pH = 4) under visible light irradiation ($\lambda \geq 400$ nm). Under the current experimental conditions, the concentration of UO_2^{2+} solution shows no obvious decrease in the absence of the photocatalysts, indicating that UO_2^{2+} is photostable and the self-photolysis process can be ignored. In dark adsorption experiments, the UO_2^{2+} ion concentration first decreased then remained constant after 60 min, indicating that the adsorption–desorption equilibrium was reached.[48,49] As displayed in Fig. S11,† the surfaces of all the samples are negatively charged at pH = 4 by zeta potential tests. As shown in Fig. S6a,† about 3% of U(VI) was removed after adsorption–desorption equilibrium in the dark for one hour. Compared to the photocatalytic removal of uranium, the above process is negligible. For comparison, we tested the photocatalytic

reduction of uranium with the conjugated polymers (**PFB** and **PCB**), pure CN, polymer heterojunctions (**PFB**/CN and **PCB**/CN) and polymer–CN mixtures (**PFB**-CN and **PCB**-CN were obtained by physically mixing the two semiconductors) under the same conditions. Regrettably, **PFB** and **PCB** did not show any photocatalytic activities. As for CN, the photocatalytic UO_2^{2+} removal efficiency was 62.8% after visible-light irradiation for 60 min and the corresponding photoreaction rate constant (k) was 0.015 min^{-1}. Unfortunately, the activities of **PFB**-CN and **PCB**-CN for the photocatalytic reduction of uranium were slightly lower than that of CN (Fig. S6b†). Excitingly, the photocatalytic activities of all the polymer heterojunctions are improved. Hereafter, we studied the relationship between polymer mass ratios and the performance of the heterojunction photocatalytic reduction of uranium. As shown in Fig. 2, both **PFB**/CN and **PCB**/CN heterojunctions achieved their highest activity for the photocatalytic reduction of uranium and maximum rate constant with the mass ratios of the polymers optimized at 5%, whereas a further increase of the polymer's mass proportion will reduce the photocatalytic activity, due to the excess polymer reducing the reaction sites of the heterojunctions.[36,38,50] Furthermore, the time-dependent variations of UO_2^{2+} concentration over CN and 5% **PFB**/CN and **PCB**/CN photocatalysts are shown in Fig. 3a. In comparison, 5% **PFB**/CN showed a significantly higher photocatalytic activity, and the photocatalytic UO_2^{2+} removal efficiency was 91.3% after visible-light irradiation for 60 min. It is worth noting that UO_2^{2+} is almost completely reduced when the illumination time is extended to 120 min, since the introduction of a carbazole unit into the D–A conjugated polymer backbone produces a stronger ICT process, resulting in improved visible light capture capability (Fig. 5) and photo-generated carrier separation efficiency of **PCB**/CN

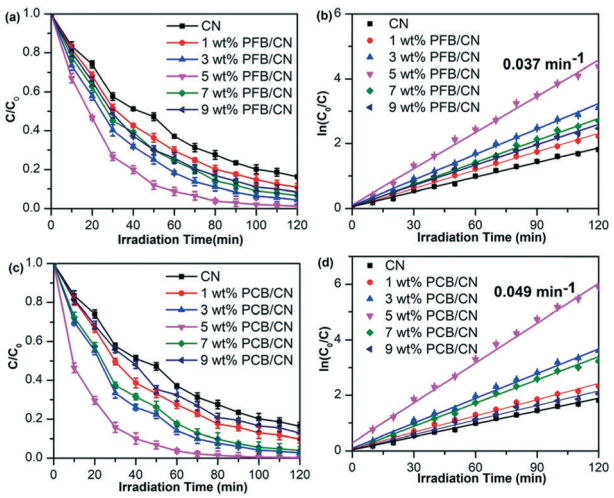

Fig. 2 (a) and (c) The variation of UO_2^{2+} concentration *vs.* illumination time of X **PFB**/CN and X **PCB**/CN; (b) and (d) the rate constant (k) of UO_2^{2+} reduction of X **PFB**/CN and X **PCB**/CN. Reaction conditions: 100 mL water containing 100 ppm U(VI) at pH 4.0, 50 mg of the photocatalysts under visible-light (400 nm ≤ λ).

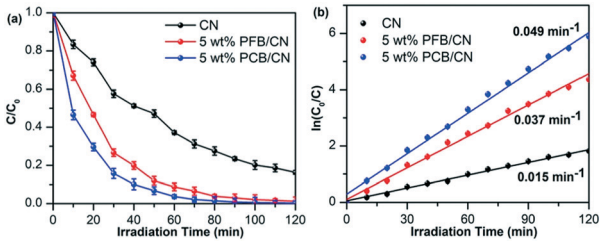

Fig. 3 (a) The variation of UO_2^{2+} concentration *vs.* illumination time of 5% **PFB**/CN and 5% **PCB**/CN; (b) the rate constant of UO_2^{2+} reduction of 5% **PFB**/CN and 5% **PCB**/CN. Reaction conditions: 100 mL water containing 100 ppm U(VI) at pH 4.0, 50 mg of the photocatalysts under visible-light (400 nm ≤ λ).

(Fig. 6). In particular, as shown in Fig. 3b, the k of **PCB**/CN is 0.049 min^{-1} according to the pseudo-first-order equation, which was 1.32 and 3.27 times higher than that of **PFB**/CN (0.037 min^{-1}) and CN (0.015 min^{-1}).

Besides the photocatalytic activity, the reusability of photocatalysts in the photocatalytic reduction process is also important for future industrialization. The reusability of **PFB**/CN and **PCB**/CN was probed by the photocatalytic reduction of UO_2^{2+} for three cycles. After each cycle run, **PFB**/CN and **PCB**/CN were recycled by centrifugation and then washed with a 1 mol L^{-1} HNO_3 solution to desorb the deposited uranium on the material surface, and hereafter washed with deionized water. Finally, the photocatalysts were dried at 80 °C in a vacuum oven for 24 h for the next UO_2^{2+} reduction experiment. As shown in Fig. 4a and b, after the three-cycle operation, the removal rate of U(VI) was only slightly reduced under visible-light irradiation, indicating that the **PFB**/CN

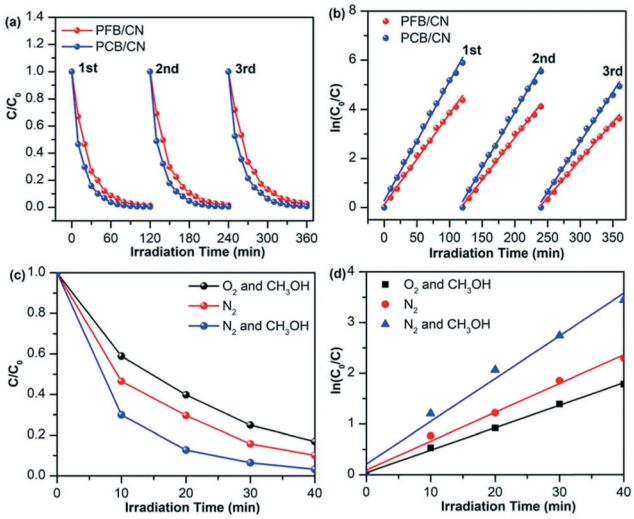

Fig. 4 Cycling performance of **PFB**/CN (a) and **PCB**/CN (b) for U(VI) photoreduction under visible-light irradiation; (c) the variation of UO_2^{2+} concentration *vs.* illumination time over the 5% **PCB**/CN photocatalyst with N_2, O_2 and/or methanol in the system; (d) the rate constant of 5% **PCB**/CN for UO_2^{2+} reduction with N_2, O_2 and/or methanol in the system. Reaction conditions: 100 mL water containing 100 ppm U(VI) at pH 4.0, 50 mg of the photocatalysts under visible-light (400 nm ≤ λ).

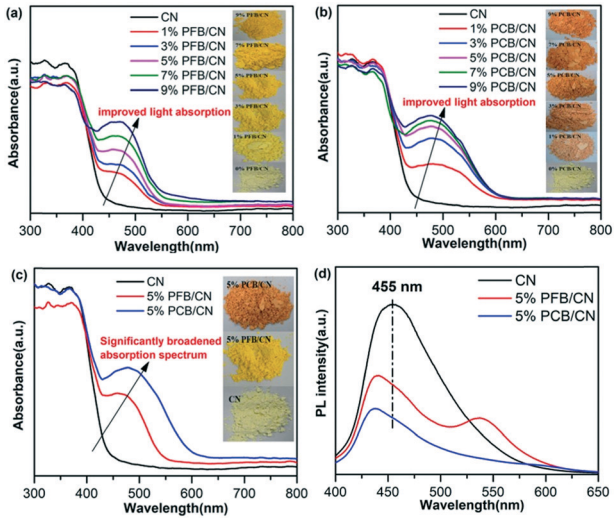

Fig. 5 (a) UV-vis diffuse reflectance spectra of X-**PFB**/CN; (b) UV-vis diffuse reflectance spectra of X-**PCB**/CN; (c) UV-vis diffuse reflectance spectra of 5% **PFB**/CN and 5% **PCB**/CN; (d) photoluminescence spectra of CN, 5% **PFB**/CN and 5% **PCB**/CN.

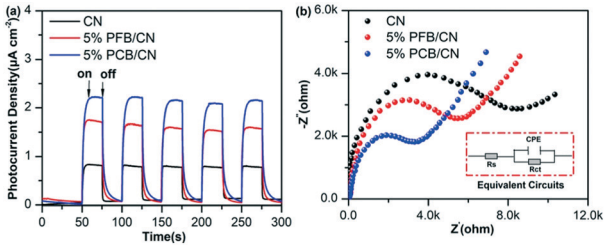

Fig. 6 (a) Transient current responses to on–off cycles of illumination on CN, 5% **PFB**/CN and 5% **PCB**/CN membrane electrodes, respectively (0 bias); (b) EIS Nyquist plots of CN, 5% **PFB**/CN and 5% **PCB**/CN at open circuit voltage.

and **PCB**/CN photocatalysts display perfect stability for the U(VI) photoreduction. This is important for future industrialization. Furthermore, FT-IR and XRD were performed on the recovered **PFB**/CN and **PCB**/CN, and the result indicates that the structure remains complete after the photocatalytic reaction (Fig.S7†). The above experimental results show that such D–A type organic conjugated polymer/CN heterostructures can be considered as a promising candidate photocatalyst for efficient photocatalytic reduction and removal of U(VI).

In general, the effective utilization of photogenerated electrons plays an important role in the photoreduction reaction of UO_2^{2+}. Compared with the reduction potential of $O_2/^{\bullet}O_2^{-}$(−0.33 V), the CB position of **PCB**/CN is more negative. O_2 and photogenerated holes (h^+) will limit the activity of the photocatalyst. As shown in Fig. 4c and d, when O_2 was saturated during photoreduction with methanol as the h^+ scavenger, the photocatalytic UO_2^{2+} removal efficiency was 83.1% within 40 min with **PCB**/CN after visible-light irradiation. When N_2 was used instead of O_2, the corresponding photocatalytic UO_2^{2+} removal efficiency was significantly increased to 96.8%, indicating that the photogenerated electron was consumed by O_2 ($O_2 + e^- \rightarrow {}^{\bullet}O_2^-$). Moreover, when the reaction was performed in a N_2 atmosphere without methanol, the removal efficiency of UO_2^{2+} was reduced to 89.9%, indicating that methanol can be used as an h^+ to enhance the separation of photo-generated carriers, thereby improving the photocatalysis of U(VI) reduction. The above experimental results confirmed that the photoexcited electrons directly participated in the photocatalytic reduction of U(VI) in an anaerobic atmosphere.

To further explain the reasons for the increase in photocatalytic activity, optical properties and interface electron transfer kinetics of the heterojunctions were investigated. Fig. 5a and b show the DRS spectra of X-**PFB**/CN and X-**PCB**/CN. Interestingly, the absorption intensity was gradually enhanced with increasing amounts of **PFB** (**PCB**) in **PFB**/CN (**PCB**/CN), especially in the region of λ = 460–600 nm, which was related to the optical absorption of **PFB** (**PCB**) in the visible light region. Compared to CN, the light absorption edges of 5% **PFB**/CN and 5% **PCB**/CN display obvious bathochromic shifts of 94 nm and 152 nm, respectively, and their corresponding colors vary from light yellow to orange (Fig. 5c). Photoluminescence (PL) emission spectra, photoelectrochemical (PEC) *I–t* curves and electrochemical impedance spectra (EIS) of the photocatalysts were thus measured. As shown in Fig. S8,† **PFB** exhibited two characteristic emission peaks at 433 nm and 556 nm, respectively. Among them, the higher energy emission peak was assigned to the donor group and the lower energy emission peak was generated by the ICT process. Comparatively, the lower energy emission peak (602 nm) of **PCB** has a significant red shift with lower fluorescence intensity, proving that the introduction of a stronger electron donor unit into the D–A conjugated polymer skeleton could facilitate exciton separation and migration. Interestingly, it can be seen from Fig. 5d that CN has a strong PL peak at 455 nm, which is attributed to the fast photo-generated carrier recombination. Obviously, the PL intensities of both the polymers and CN significantly decreased when they form the polymer/CN heterojunction. This means that CN and **PFB** (**PCB**) can suppress the photo-generated recombination with each other, which is a strong indication of the efficient charge transfer between the polymers and CN. In addition, the PL peaks of CN and the polymers are blue shifted after forming polymer/CN. This is possibly because of the π–π intermolecular interaction decreasing the interchain interactions within CN and the polymers. Besides, as seen from Fig. 6a, the transient photocurrent responses of the polymer/CN heterojunctions are profoundly strengthened compared to that of CN under visible-light illumination, and **PCB**/CN displays the maximum photocurrent density of 2.22 μA cm^{-2}, which is about 1.27 and 2.67 times higher than that of **PFB**/CN and CN, respectively, indicating the increased electron and hole separation ability in the **PCB**/CN heterostructure. EIS was conducted to confirm the interface charge transfer characteristics of CN, **PFB**/CN and **PCB**/CN.

In view of the Nyquist diagram and the corresponding equivalent circuit pattern in Fig. 6b, polymer/CN exhibits smaller interfacial charge transfer resistance (R_{CT}). Compared to **PFB**/CN and CN, the smallest arc radius of **PCB**/CN indicates a decreased charge transfer resistance and accelerated charge transfer. The above analysis indicates that **PCB**/CN exhibits excellent activity for the photocatalytic reduction of uranium due to its broadened visible light response range and improved e^-/h^+ separation ability.

In order to further clarify the interaction mechanism between UO_2^{2+} and the heterojunction photocatalysts, the U4f XPS spectra of polymer/CN with different photoreduction times were obtained (Fig. 7). For **PFB**/CN without light irradiation (0 min), two distinct characteristic peaks at 393.0 and 382.1 eV were attributed to $U4f_{5/2}$ and $U4f_{7/2}$ of U(VI), respectively (Fig. 7a), because a certain amount of UO_2^{2+} is adsorbed on the surface of the sample.[51–54] Meanwhile, the peaks at 392.4 and 381.6 eV were found after 60 min of the photocatalytic reaction, which were attributed to $U4f_{5/2}$ and $U4f_{7/2}$ of U(IV), respectively, indicating that hexavalent uranium was effectively reduced to uranium dioxide. It is worth noting that as the reaction time was extended from 60 min to 120 min, the U(IV)/U(VI) ratio was increased from 0.44 to 1.45. In comparison, the ratio of U(IV)/U(VI) of **PCB**/CN increased more obviously with the extension of the irradiation time. For **PCB**/CN with 120 min of irradiation, almost all of the hexavalent uranium is reduced to tetravalent uranium, indicating its perfect photocatalytic performance (Fig. 7b). In addition, the SEM image of the heterojunction photocatalysts after the reaction and the corresponding EDS mappings are shown in Fig. 8. After the photocatalytic reaction, the morphology of the heterojunction photocatalysts did not change significantly, indicating that they have good mechanical stability. As seen from the corresponding mappings, the constituent elements of the photocatalysts after the reaction included C, N, O, S and U, which indicates that the surface of the photocatalyst is loaded with uranium species after light irradiation.

Fig. 9 shows the diagrammatic sketch of the energy band structure on the basis of the above calculations and the principle of charge carrier separation in the polymer/CN heterojunctions. Since the reduction potential of UO_2^{2+} to UO_2 (UO_2^{2+}/UO_2: 0.411 V *vs.* SHE) is more positive than that of the CB bottom of the polymers and CN, therefore, the

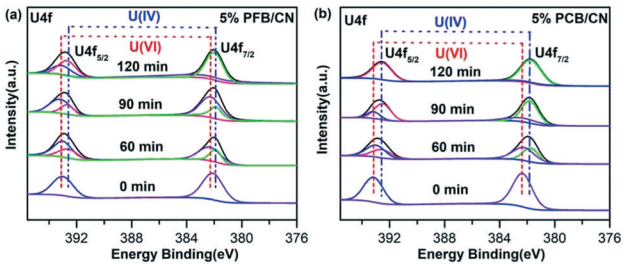

Fig. 7 U 4f XPS spectra of (a) 5% **PFB**/CN and (b) 5% **PCB**/CN after different reaction times.

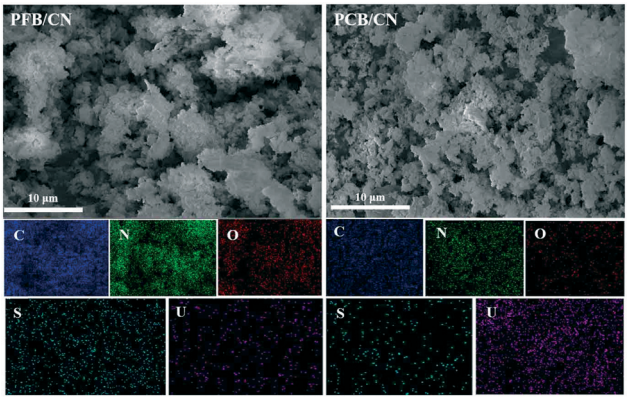

Fig. 8 The SEM images of 5% **PFB**/CN and 5% **PCB**/CN after the reaction and the corresponding EDS mappings. Scale bar: 10 μm.

polymer/CN photocatalytic reduction of uranium is thermodynamically feasible. Furthermore, the band alignment between CN and **PFB** (**PCB**) suggests that it has a typical type II heterojunction structure. Driven by the type II band alignment between the polymers and CN, the photoexcited electrons situated in the CB of the polymers would transfer to the CB of CN, and then directly migrate to the surface for the photocatalytic reduction of uranium ions, and at the same time, the photogenerated holes in CN would soon move to the VB of the polymers and then participate in the oxidation reaction, thus resulting in efficient photogenerated carrier separation in polymer/CN. In addition, at the interface of the two semiconductors, electrons accumulate in the CN region and holes accumulate in the polymer region, thereby generating a polarized built-in electric field at the interface, which can suppress photocarrier recombination and greatly promote the separation of e^-/h^+ pairs, leading to the enhanced activity for the photocatalytic reduction of uranium.

In order to deeply inspect the effect of the introduction of N atoms into the donor unit of the polymer skeleton of the polymer/heterojunction on the performance for the

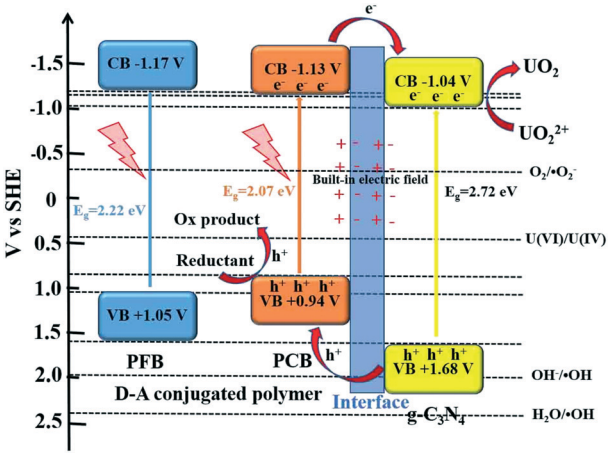

Fig. 9 Proposed photocatalytic uranium reduction mechanism of **PFB**/CN and **PCB**/CN.

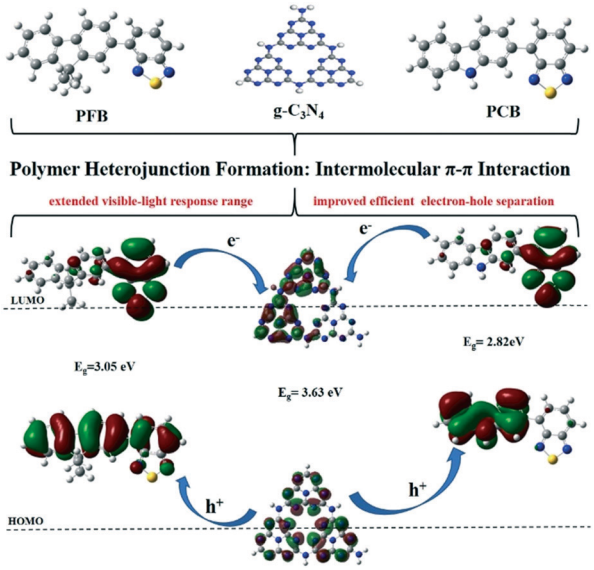

Fig. 10 Theoretical calculations are used to explain the enhancement of the photocatalytic activity of **PFB**/CN and **PCB**/CN.

photocatalytic reduction of uranium, density functional theory (DFT) calculations of CN, **PFB** and **PCB** were carried out. According to the distribution of the frontier molecular orbitals, D–A conjugated polymers **PFB** and **PCB** show a high degree of HOMO–LUMO separation (Fig. S9†), suggesting that there is intramolecular charge transfer (ICT) in the polymer backbone. As shown in Fig. S10,† the Mulliken charge quantitative analysis for **PFB** and **PCB** were carried out. The results showed that there were 0.246 e and 0.440 e transferred from donor to acceptor in the **PFB** and **PCB** polymer skeleton, respectively. Therefore, the introduction of nitrogen atoms in the donor unit of the polymer skeletons significantly enhanced the ICT process, which further promoted the Frenkel exciton dissociation and widened the visible light response range. As can be seen from Fig. 10, **PFB**/CN (**PCB**/CN) was favourably acquired through the π–π interaction of **PFB** (**PCB**) and CN. Driven by the type II band alignment between the polymers and CN, the photogenerated electrons in the polymers would transfer to the LUMO of CN and then migrate to the surface for the photocatalytic reduction of uranium; while the photogenerated holes in CN would move to the HOMO of the polymers, thus leading to an extended visible-light response range, improved electron–hole separation, and efficient photocatalytic reduction of uranium.

Conclusions

In summary, D–A conjugated polymer/CN heterojunction photocatalysts were successfully constructed for stable and efficient photocatalytic reduction of uranium under visible light irradiation. A heteroatomic engineering strategy was innovatively proposed toward higher photocatalytic activities, by modification of the polymer molecular structure to improve visible light capture capability and promote the separation efficiency of photogenerated electron–hole pairs of polymer/CN. It was revealed that copolymerization of a nitrogen-containing electron donor carbazole unit into the polymer backbone would widen the light response range and promote electron–hole separation within the formed **PCB**/CN as compared to **PFB**/CN, thus achieving a significantly improved activity for the photocatalytic reduction of uranium; the photocatalytic UO_2^{2+} removal rate was 96.3% after visible-light irradiation for 60 min and UO_2^{2+} was almost completely reduced when the illumination time was extended to 120 min. The corresponding k value is 0.049 min^{-1}. The present findings open up a novel way to modify the electronic structure of polymer heterojunction photocatalysts for efficient removal of uranium in nuclear waste through rational molecular design. What's more, the efficient and stable photocatalytic reduction of uranium makes them have excellent potential in real environmental pollution clean-up.

Conflicts of interest

There are no conflicts to declare.

Acknowledgements

We thank the National Science Foundation of China (21966002, 21871047, 21661001, and 21661002) and the Natural Science Foundation of Jiangxi Province of China (20181ACB20003).

Notes and references

1 A. Keshtkar, M. Mohammadi and M. Moosavian, *J. Radioanal. Nucl. Chem.*, 2015, **303**, 363–376.
2 M. Manos and M. Kanatzidis, *J. Am. Chem. Soc.*, 2012, **134**, 16441–16446.
3 J. Li, X. Wang, G. Zhao, C. Chen, Z. Chai, A. Alsaedi, T. Hayat and X. Wang, *Chem. Soc. Rev.*, 2018, **47**, 2322–2356.
4 M. J. Manos and M. G. Kanatzidis, *J. Am. Chem. Soc.*, 2012, **134**, 16441–16446.
5 X. Wang, L. Chen, L. Wang, Q. Fan, D. Pan, J. Li, F. Chi, Y. Xie, S. Yu, C. Xiao, F. Luo, J. Wang, X. Wang, C. Chen, W. Wu, W. Shi, S. Wang and X. Wang, *Sci. China: Chem.*, 2019, **62**, 933–967.
6 X. Xiong, Z. Yu, L. Gong, Y. Tao, Z. Gao, L. Wang, W. Yin, L. Yang and F. Luo, *Adv. Sci.*, 2019, **6**, 1900547.
7 L. Zhang, L. Wang, L. Gong, X. Feng, M. Luo and F. Luo, *J. Hazard. Mater.*, 2016, **311**, 30–36.
8 J. Li, L. Gong, X. Feng, L. Zhang, H. Wu, C. Yan, Y. Xiong, H. Gao and F. Luo, *Chem. Eng. J.*, 2016, **302**, 763–772.
9 T. A. Saleh, Naeemullah, M. Tuzen and A. Sarl, *Chem. Eng. Res. Des.*, 2017, **117**, 218–227.
10 F. Zare, M. Ghaedi, A. Daneshfar, S. Agarwal, I. Tyagi, T. A. Saleh and V. K. Gupta, *Chem. Eng. J.*, 2015, **273**, 296–306.
11 S. Yan, B. Hua, Z. Bao, J. Yang, C. Liu and B. Deng, *Environ. Sci. Technol.*, 2010, **44**, 7783–7789.
12 Y. Zhao, C. Tao, G. Xiao, G. Wei, L. Li, C. Liu and H. Su, *Nanoscale*, 2016, **8**, 5313–5326.

13 X. Wang, K. Maeda, A. Thomas, K. Takanabe, G. Xin, J. M. Carlsson, K. Domen and M. Antonietti, *Nat. Mater.*, 2009, **8**, 76–80.
14 X. Li, J. Xiong, X. Gao, J. Huang, Z. Feng, Z. Chen and Y. Zhu, *J. Alloys Compd.*, 2019, **802**, 196–209.
15 X. Li, J. Xiong, Y. Xu, Z. Feng and J. Huang, *Chin. J. Catal.*, 2019, **40**, 424–433.
16 (*a*) F. T. Yu, Z. Q. Wang, S. C. Zhang, K. Yun, H. N. Ye, X. Q. Gong, J. L. Hua and H. Tian, *Appl. Catal., B*, 2018, **220**, 542–552; (*b*) K. L. Corp and C. W. Schlenker, *J. Am. Chem. Soc.*, 2017, **139**, 790–47912; (*c*) M. Wang, P. Ju, J. J. Li, Y. Zhao, X. X. Han and Z. M. Ha, *ACS Sustainable Chem. Eng.*, 2017, **5**, 7878–7886.
17 C. Lu, R. Chen, X. Wu, M. Fan, Y. Liu, Z. Le, S. Jiang and S. Song, *Appl. Surf. Sci.*, 2016, **360**, 1016–1022.
18 C. Lu, P. Zhang, S. Jiang, X. Wu, S. Song, M. Zhu, Z. Lou, Z. Li, F. Liu, Y. Liu, Y. Wang and Z. Le, *Appl. Catal., B*, 2017, **200**, 378–385.
19 A. Kudo and Y. Miseki, *Chem. Soc. Rev.*, 2009, **38**, 253–278.
20 J. Yu, S. Wang, J. Low and W. Xiao, *Phys. Chem. Chem. Phys.*, 2013, **15**, 16883–16890.
21 X. She, J. Wu, H. Xu, J. Zhong, Y. Wang, Y. Song, K. Nie, Y. Liu, Y. Yang, M. Rodrigues, R. Vajtai, J. Lou, D. Du, H. Li and P. Ajayan, *Adv. Energy Mater.*, 2017, **8**, 1700025–1700031.
22 K. Sridharan, E. Jang and T. Park, *Appl. Catal., B*, 2013, **142**, 718–728.
23 (*a*) R. Sprick, B. Bonillo, R. Clowes, P. Guiglion, N. Brownbill, B. Slater, F. Blanc, M. Zwijnenburg, D. Adams and A. Cooper, *Angew. Chem., Int. Ed.*, 2016, **55**, 1792–1796; (*b*) J. Xu, S. M. Bi, W. Q. Tang, Q. Kang, D. F. Niu, S. Z. Hu, S. L. Zhao, L. M. Wang, Z. Xin and X. S. Zhang, *J. Mater. Chem. A*, 2019, **7**, 18100–18108.
24 P. Pati, G. Damas, L. Tian, D. Fernandes, L. Zhang, I. Pehlivan, T. Edvinsson, C. Araujo and H. Tian, *Energy Environ. Sci.*, 2017, **10**, 1372–1376.
25 L. Wang, L. Tian, H. Chen and H. Tian, *Angew. Chem., Int. Ed.*, 2016, **55**, 12306–12310.
26 Z. Lan, W. Ren, X. Chen, Y. Zhang and X. Wang, *Appl. Catal., B*, 2019, **245**, 596–603.
27 R. Sprick, Y. Bai, A. Guilbert, M. Zbiri, C. Aitchison, L. Wilbraham, Y. Yan, D. Woods, M. Zwijnenburg and A. Cooper, *Chem. Mater.*, 2019, **31**, 305–313.
28 R. Sprick, B. Bonillo, R. Clowes, P. Guiglion, N. Brownbill, B. Slater, F. Blanc, M. Zwijnenburg, D. Adams and A. Cooper, *Angew. Chem.*, 2016, **128**, 1824–1828.
29 F. T. Yu, Z. Q. Wang, S. C. Zhang, H. N. Ye, K. Y. Kong, X. Q. Gong, J. L. Hua and H. Tian, *Adv. Funct. Mater.*, 2018, **28**, 1804512–1804524.
30 X. Chen, S. Shen, L. Guo and S. Mao, *Chem. Rev.*, 2010, **110**, 6503–6570.
31 W. Hehre, R. Ditchfield and J. Pople, *J. Chem. Phys.*, 1972, **56**, 2257–2261.
32 J. Chen, C. Dong, D. Zhao, Y. Huang, X. Wang, L. Samad, L. Dang, M. Shearer, S. Shen and L. Guo, *Adv. Mater.*, 2017, **29**, 1606198–1606208.
33 L. Yao, D. Wei, Y. Ni, D. Yan and C. Hu, *Nano Energy*, 2016, **26**, 248–256.
34 X. She, H. Xu, Y. Xu, J. Yan, J. Xia, L. Xu, Y. Song, Y. Jiang, Q. Zhang and H. Li, *J. Mater. Chem. A*, 2014, **2**, 2563–2570.
35 T. A. Saleh, *J. Water Supply: Res. Technol.–AQUA*, 2015, **64**, 892–903.
36 T. A. Saleh, *Desalin. Water Treat.*, 2015, **57**, 10730–10744.
37 T. A. Saleh, *Environ. Sci. Pollut. Res.*, 2015, **22**, 16721–16731.
38 T. A. Saleh, *J. Cleaner Prod.*, 2018, **172**, 2123–2132.
39 T. A. Saleh, K. O. Sulaiman and S. A. AL-Hammadi, *Appl. Catal., B*, 2020, **263**, 117661.
40 W. Zhen, X. Ning, B. Yang, Y. Wu, Z. Li and G. Lu, *Appl. Catal., B.*, 2018, **221**, 243–257.
41 W. Yang, L. Zhang, J. Xie, X. Zhang, Q. Liu, T. Yao, S. Wei, Q. Zhang and Y. Xie, *Angew. Chem., Int. Ed.*, 2016, **55**, 6716–6720.
42 J. Zhang, M. Zhang, R. Sun and X. Wang, *Angew. Chem.*, 2012, **124**, 10292–10296.
43 J. Yan, H. Wu, H. Chen, Y. Zhang, F. Zhang and S. Liu, *Appl. Catal., B.*, 2016, **191**, 130–137.
44 K. Kong, S. Zhang, Y. Chu, Y. Hu, F. Yu, H. Ye, H. Ding and J. Hua, *Chem. Commun.*, 2019, **55**, 8090–8093.
45 Z. Zhang, Y. Zhu, X. Chen, H. Zhang and J. Wang, *Adv. Mater.*, 2018, **31**, 1806626–1806631.
46 J. Wang, W. Shi, D. Liu, Z. Zhang, Y. Zhu and D. Wang, *Appl. Catal., B.*, 2017, **202**, 289–297.
47 M. Wen, J. Wang, R. Tong, D. Liu, H. Huang, Y. Yu, Z. Zhou, P. Chu and X. Yu, *Adv. Sci.*, 2019, **6**, 1801321–1801327.
48 T. A. Saleh and A. A. Al-saadi, *Surf. Interface Anal.*, 2015, **47**, 785–792.
49 T. A. Saleh, A. A. Al-saadi and V. K. Gupta, *J. Mol. Liq.*, 2014, **191**, 85–91.
50 F. He, G. Chen, Y. Yu, S. Hao, Y. Zhou and Y. Zheng, *ACS Appl. Mater. Interfaces*, 2014, **6**, 7171–7179.
51 J. Li, Z. Huang, W. Guo, L. Wang, L. Zheng, Z. Chai and W. Shi, *Environ. Sci. Technol.*, 2017, **51**, 5666–5674.
52 H. Wang, H. Guo, N. Zhang, Z. Chen, B. Hu and X. Wang, *Environ. Sci. Technol.*, 2019, **53**, 6454–6461.
53 H. Deng, Z. Li, L. Wang, L. Yuan, J. Lan, Z. Chang, Z. Chai and W. Shi, *ACS Appl. Nano Mater.*, 2019, **24**, 2283–2294.
54 X. Jiang, Q. Xing, X. Luo, F. Li, J. Zou, S. Liu, X. Li and X. Wang, *Appl. Catal., B.*, 2018, **202**, 29–38.